Dalton Transactions

PAPER

View Article Online
View Journal | View Issue

Cite this: *Dalton Trans.*, 2017, **46**, 369

The mechanism of selective catalytic reduction of NO_x on Cu-SSZ-13 – a computational study†

Douglas W. Crandell,[a] Haiyang Zhu,[b] Xiaofan Yang,*[b] John Hochmuth[b] and Mu-Hyun Baik*[a,c,d]

Received 9th October 2016,
Accepted 28th November 2016

DOI: 10.1039/c6dt03894h

www.rsc.org/dalton

The copper-exchanged aluminosilicate zeolite SSZ-13 is a leading catalyst for the selective catalytic reduction of NO. Density functional theory calculations are used to construct a complete catalytic cycle of this process paying special attention to the coordination geometries and redox states of copper. N_2 can be produced in the reduction half-cycle *via* a nitrosamine intermediate generated from the reaction of the additive reductant NH_3 with a NO^+ intermediate stabilized by the zeolite lattice. The decomposition of this nitrosamine species can be assisted by incipient Brønsted acid sites generated during catalysis. Our calculations also suggest that the reoxidation of Cu(I) to Cu(II) requires the addition of both NO and O_2. The production of a second equivalent of N_2 during the oxidation half-cycle proceeds through a peroxynitrite intermediate to form a Cu–nitrite intermediate, which may react with an acid, either HNO_2 or NH_4^+ to close the catalytic cycle. Models of copper neutralized by an external hydroxide ligand are also examined. These calculations form a key basis for understanding the mechanism of NO reduction in Cu-SSZ-13 in order to develop strategies for rationally optimizing the performance in future experiments.

Introduction

The selective catalytic reduction (SCR) of NO_x to N_2 using NH_3 as the sacrificial oxidant is a promising technology that may allow for eliminating hazardous NO_x from lean-burn engine exhaust in a highly energy economical way.[1–5] In this process NH_3 reacts selectively with NO over O_2 to produce N_2 and water vapor (eqn (1)).

$$4\ NH_3 + 4\ NO + O_2 \rightarrow 4\ N_2 + 6H_2O \quad (1)$$

The leading technology for the SCR process uses zeolites with Fe and Cu ions exchange-deposited into the zeolite matrix that offer better hydrothermal stability compared to metal oxides,[6,7] such as V_2O_5,[8–10] and operates at a wider range of temperatures, in addition to offering higher NO_x conversion efficiency at low temperatures.[11] Among the best of these zeolite-supported catalysts[12–15] is the Cu-exchanged chabazite (CHA), Cu-SSZ-13, patented by the BASF company.[16]

The CHA framework consists of two silicate-based six-membered rings stacked on top of each other. These double layered six-member rings (d6r) are bridged by smaller four-membered rings to create larger eight-membered rings. Silicon atoms at tetrahedral sites in the framework can be substituted for Al to introduce anionic sites, which can bind a copper cation. A number of studies have been performed, both experimental[17–26] and computational,[27–32] that have attempted to elucidate the nature of the active site of this catalyst. It is generally accepted that Cu^{2+} atoms are bound within the six-membered ring of the d6r subunit[33] at the active site, although some debate remains[27,34–41] as it has been suggested that Cu^{2+} may be supported by a hydroxide anion in the larger eight-membered ring or may move to the eight-membered ring upon binding NO.[42–44] The mechanism of the SCR reaction is not well understood, making it difficult to incorporate rational design strategies for improving catalyst performance.

Although copper is initially bound as Cu(II), XAS data suggest that Cu(II) is reduced to Cu(I) under standard SCR conditions.[27,45] Diffuse Reflectance Infrared Fourier Transform spectroscopy (DRIFTs) and NMR studies have provided evidence for the formation of a possible NO^+–Cu^+ intermediate.[28,38,46] We have previously studied a number of possible intermediates in the SCR catalytic cycle using computational molecular modeling techniques and have identified a structure of a potential NO^+ intermediate where the NO^+ substrate is supported by the negative charge delocalized throughout the Al-doped chabazite.[46] An alternative proposal suggests that both NH_3 and NO are necessary to reduce Cu(II) to Cu(I) and produces a proximal Brønsted

[a]*Department of Chemistry, Indiana University, 800 E. Kirkwood Avenue, Bloomington, IN 47405, USA. E-mail: mbaik2805@kaist.ac.kr*
[b]*BASF Corporation, 25 Middlesex/Essex Turnpike, Iselin, NJ 08830, USA. E-mail: xiaofan.yang@basf.com*
[c]*Center for Catalytic Hydrocarbon Functionalizations, Institute for Basic Science (IBS), Daejeon 305-701, South Korea*
[d]*Department of Chemistry, Korea Advanced Institute of Science and Technology (KAIST), Daejeon 305-701, South Korea*

†Electronic supplementary information (ESI) available. See DOI: 10.1039/c6dt03894h

acid site (H^+) along with the Cu(I)–H_2NNO nitrosamine species.[47] The proximal Brønsted acid site may recruit a molecule of NH_3 which will be used along with NO and O_2 in the oxidation half-cycle to produce N_2 and H_2O and regenerate Cu(II).

Here, we build on our previous study[46] where we corroborated potential reaction intermediates by comparing calculated vibrational modes with frequencies observed experimentally using DRIFTS, to construct a complete reaction profile for the SCR process in Cu-SSZ-13 initiated by Cu(II) engaging the substrates NO_x, NH_3 and O_2. We found that the copper ion is very mobile within the d6r subunit and can change its coordination geometry as necessary to access a variety of redox states Cu(I), Cu(II) and Cu(III). We propose that the reduction half-cycle generates a nitrosamine species, which requires the assistance of a Brønsted acid site on the zeolite to decompose into N_2 and H_2O and that a second equivalent of N_2 is produced in the oxidation half-cycle that proceeds through a peroxynitrite intermediate. This work constitutes the first report of the complete catalytic cycle of a selective catalytic reduction process under highly oxidizing conditions. Whereas many new questions are raised by our findings, it is our hope that this work provides a foundation for further discussion about the mechanism of the SCR process.

Computational

Calculations on the small cluster model of the d6r subunit of chabazite were performed using density functional theory[48,49] as implemented in the Jaguar 8.1 suite of *ab initio* quantum chemistry programs.[50] Geometry optimizations were performed at the PBE/6-31G** level of theory[51,52] with copper represented by the Los Alamos LACVP basis set,[53,54] which includes relativistic effective core potentials. More reliable single point energies were computed from the optimized geometries using Dunning's correlation-consistent triple-ζ basis set, cc-pVTZ(-f),[55] where copper was represented using a modified version of LACVP, designated as LACV3P with decontracted exponents to match the effective core potential with a triple-ζ quality basis. Vibrational frequency analysis was performed at the PBE/6-31G** level of theory to derive zero point energy and vibrational entropy corrections from unscaled frequencies. All optimized structures were confirmed to be minima on the potential energy surface by the presence of no imaginary frequencies, whereas transition state structures were confirmed as saddle points with only one imaginary frequency corresponding to the vibrational mode of interest.

The energy components have been computed with the following protocol. The free energy in gas phase G(gas) has been calculated as follows:

$$G(\text{gas}) = H(\text{gas}) - TS(\text{gas}) \quad (2)$$

$$H(\text{gas}) = E(\text{SCF}) + \text{ZPE} \quad (3)$$

$$\Delta G(\text{gas}) = \sum G(\text{gas}) \text{ for products} - \sum G(\text{gas}) \text{ for reactants} \quad (4)$$

G(gas) is the free energy in gas phase; H(gas) is the enthalpy in gas phase; T is the temperature (298 K); S(gas) is the entropy in gas phase; E(SCF) is the self-consistent field energy, *i.e.* "raw" electronic energy as computed from the SCF procedure and ZPE is the zero point energy.

Single point coupled-cluster calculations with singles, doubles, and perturbative triples CCSD(T)[56] for calculations of the overall thermodynamics of transformations of gas-phase substrates without the zeolite were performed using the ORCA quantum chemistry package[57] and using Dunning's correlation-consistent cc-pVTZ and cc-pVQZ basis sets.[55] For these reactions, the energetics of the transformations were also calculated using DFT with the M06-2X functional in addition to PBE.[58]

Results and discussion

Any mechanistic investigation of a catalytic reaction must begin with the resting state of the catalytic cycle. In our previous work a plausible resting state of the catalyst was found to consist of a Cu(II) ion bound within a d6r subunit of the chabazite that is structurally modified by two aluminate sites. The aluminum atoms are positioned diagonally in two opposite six-membered rings to minimize the electrostatic repulsion between them. Throughout the study, we characterize the basic ring structure motif as 6-membered referring only to the number of Si/Al atoms, although there are 12 atoms in the ring when the oxygen atoms are included. The optimized structure of the Cu(II) bound species **1** is shown in Fig. 1 along with selected bond lengths and angles summarized in Table 1. The copper ion adopts a distorted square planar coordination geometry in the six-membered ring, where it forms a significantly shorter bond of 1.947 Å to one of the framework oxygen atoms O1 bound to the anionic aluminate site. The angle defined by O2–Cu–O4 is nearly linear at 179.5°, but the structural constraints imposed by the silicate ring limit the O1–Cu–O3 angle to just 134.3°. This strained geometry creates an electronic driving force at the copper center to utilize the incoming NO molecule as a ligand and adopt a more relaxed coordination geometry. This binding of NO at the Cu(II) ion is exergonic

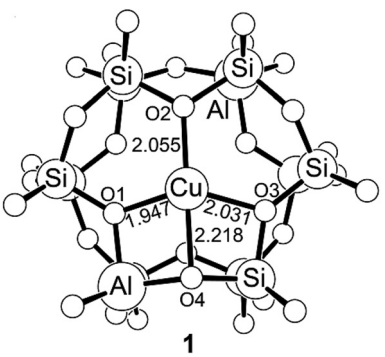

1

Fig. 1 Optimized structure of **1**.

Table 1 Selected calculated bond distances and angles for **1**

Structural parameter	Distance (Å)	Angle (°)
Cu–O1	1.947	—
Cu–O2	2.055	—
Cu–O3	2.031	—
Cu–O4	2.218	—
∠O2–Cu–O4	—	179.5
∠O1–Cu–O3	—	134.3

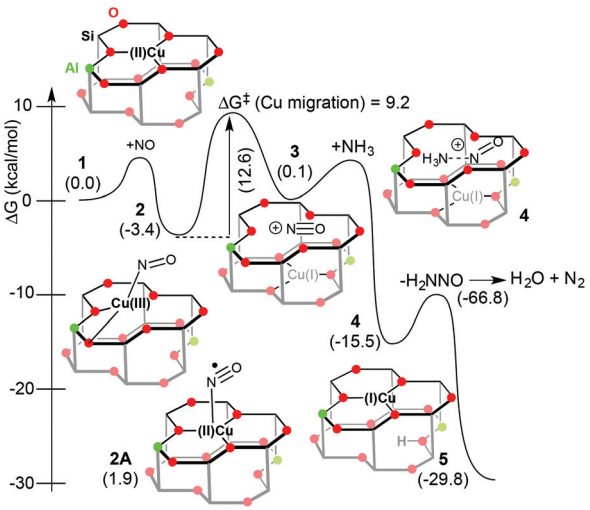

Fig. 2 Mechanism of the reduction half-cycle in NO_x reduction by Cu-SSZ-13. Relative energies in kcal mol^{-1} are given in parenthesis.

with a free energy of −3.4 kcal mol^{-1} and gives complex **2**, which starts the catalytic reduction cycle, as shown in Fig. 2. In intermediate **2** the copper center assumes a trigonal planar structure and is slightly displaced from the molecular plane. The NO ligand is inherently redox-active in the sense that it can bind to a metal formally as NO^+, NO or NO^-. Changes in oxidation state of the NO ligand will of course be accompanied by corresponding changes of the metal oxidation state, which in turn will determine which chemical transformations are viable at each step in the mechanism. The simplest case involves forming a standard Lewis acid–base adduct between Cu and NO, where no electron transfer takes place and the copper maintains an oxidation state of +II. Our calculations show that there is no significant spin density on either the copper ion or the nitrosyl fragment and the Cu–N–O moiety displays a bond angle of 156.3°. Taken together, these results suggest that the copper has been oxidized during NO binding and the electronic structure of complex **2** is most consistent with that of a Cu(III) center carrying an anionic NO^- ligand. We located an alternative adduct structure **2A**, where copper maintains a trigonal planar coordination geometry with the framework oxygen atoms of the zeolite lattice and the nitrosyl radical forms a weak interaction through the lone pair orbitals on nitrogen at a distance of 2.640 Å. This adduct structure **2A**, is 5.3 kcal mol^{-1} higher in energy than **2** and mechanistically irrelevant.

To push the catalytic cycle forward, intermediate **2** must undergo formally a reductive elimination at a minimal thermodynamic cost of 3.3 kcal mol^{-1} traversing a reasonable barrier of 12.6 kcal mol^{-1} to generate intermediate **3**, which contains a NO^+ moiety that is no longer bound to copper, but remains trapped in the zeolite cage. The reduced metal center Cu(I) migrated across the d6r subunit and is bound to the second six-membered silicate ring, as illustrated in Fig. 2. In absence of ammonia, this species should display a finite lifetime. In our previous work, this intermediate was identified as being responsible for the unusual vibrational signature at the frequency of 2170 cm^{-1} detected in the DRIFTs experiment. Our calculation assigned a frequency of 2159 cm^{-1} to the N–O stretching mode of this species, constituting a good agreement between the experimental and computational vibrational spectra. As pointed out previously, such a high energy stretching frequency is not compatible with a neutral or metal bound NO fragment and strongly supports our proposal of a free floating NO^+ moiety within the zeolite cage, which presents a delocalized, negative electrostatic potential due to the Al-doping.

Given the shortened N–O bond length in **2** of 1.143 Å compared to 1.170 Å found for the free NO along with a ∠Cu–N–O angle of 156.3°, it is reasonable to view intermediate **2** as to contain an anionic nitrosyl ligand bound to a formally Cu(III)-center. Thus, the NO binds to the Cu(II) center in an oxidative fashion and becomes an anionic nitrosyl ligand interacting fairly strongly with a freshly oxidized Cu(III) ion. Within this interpretation, the rearrangement of **2** to form species **3** formally constitutes a reductive elimination of the nitrosyl ligand, where the formally anionic NO^- fragment transfers two electrons to the Cu(III) center to generate Cu(I) and NO^+.

The cationic NO^+ fragment in intermediate **3** is likely to be highly reactive towards nucleophiles, such as NH_3. Fig. 3

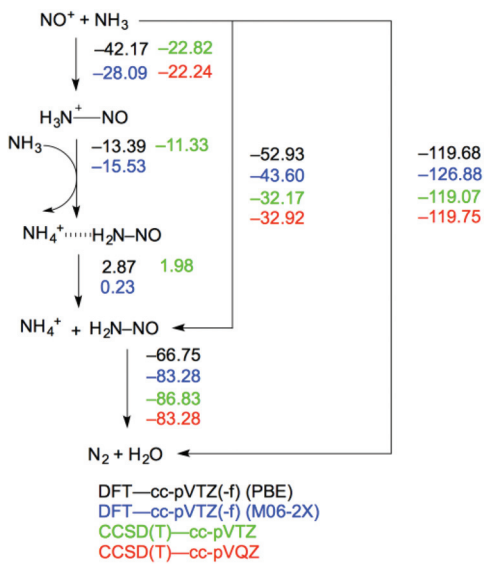

Fig. 3 Thermodynamics in kcal mol^{-1} for the formation of protonated nitrosamine from NO^+ and NH_3 along with subsequent decomposition into N_2 and H_2O with no zeolite involvement calculated with DFT and CCSD(T).

shows the calculated thermodynamics of the reaction of NO^+ with NH_3 along with the subsequent decomposition of the formed nitrosamine species into N_2 and H_2O without involvement of the zeolite. The overall energy of these processes is calculated to be −119.75 kcal mol^{-1} at the CCSD(T)/cc-pVQZ level of theory, which can be considered to be a much more accurate method than the computationally efficient, but approximate DFT calculations. Unfortunately, the computational cost quickly becomes intractable at the CCSD(T)/cc-pVQZ level. The comparison of the different computational methods highlight that the DFT, in particular when the popular M06-2X functional is used, provides a reasonable agreement with the higher levels of theory at a fraction of its computational cost. For example, the overall driving force of the reaction between NO^+ and 2 NH_3 to form NH_4^+, N_2 and H_2O is predicted to be −119.75 kcal mol^{-1} at the highest level of theory, CCSD(T)/cc-pVQZ, while the much more economical DFT calculations give −119.68 and −126.88 kcal mol^{-1}, as illustrated in Fig. 3. The energies of the intermediates are also reproduced within a reasonable range. It is unsurprising that the M06-2X functional, which is parameterized for nonmetals and to handle dispersion interactions performs better than PBE on the initial N–N bond forming step between NO^+ and NH_3 and the final dissociation step to form N_2 and H_2O. Nevertheless, PBE provides a good enough agreement with the energies from the coupled-cluster calculations to construct a plausible mechanism for the reaction upon including both the copper and Al-doped zeolite.

When the zeolite interacts with the substrate, forming the nitrosammonium adduct **4** is favorable by 15.6 kcal mol^{-1}, as illustrated in Fig. 2. This energy is reasonable, since the formation of the nitrosamine product from the substrates is downhill by 83.3 kcal mol^{-1}, as shown in Fig. 3. The nitrosammonium cation can donate a proton to one of the aluminate sites in the d6r subunit and subsequently decompose to N_2 and H_2O producing a Cu(I) center to complete the first reduction half-reaction cycle. The Cu(I) ion is bound in one of the six-membered rings **5** with a Brønsted acidic site on one of the zeolite framework oxygen atoms to neutralize the charge of the additional aluminate site.

Despite a substantial thermodynamic driving force for producing N_2 and H_2O from H_2N–NO, the reaction is kinetically very challenging and high reaction barriers must be overcome in order to accomplish this transformation. To better understand what the catalysis has to accomplish, it is instructional to consider the energies of the uncatalyzed analogue. The putative uncatalyzed reaction of nitrosamine decomposing to afford dinitrogen and water was calculated at the CCSD(T)/cc-pVQZ level of theory and the reaction energies are summarized in Fig. 4. The most viable reaction pathway involves the transfer of the amine proton to the oxo of the nitroso group to form the *trans*-hydroxydiimide **C** traversing the transition state **TS2** at 31.4 kcal mol^{-1}. Alternatively, transferring the proton to the nitrogen atom of the nitroso group yields the diimide *N*-oxide **B**. Our calculations place this intermediate at 10.1 kcal mol^{-1} and gives a prohibitively high barrier **TS1** of 60.4 kcal mol^{-1}.

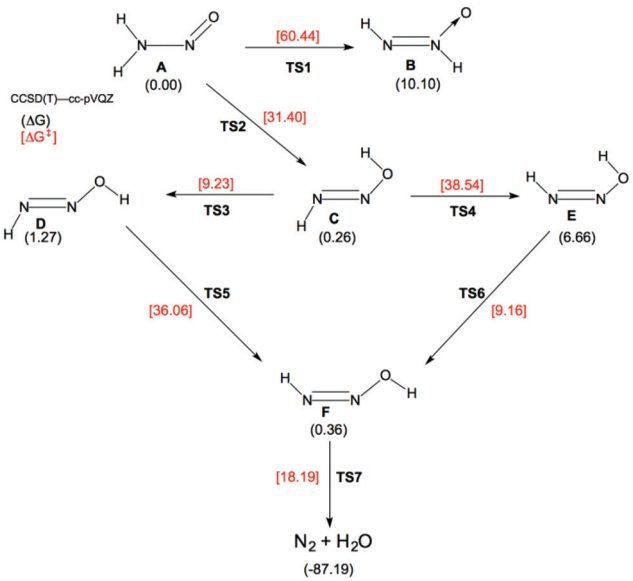

Fig. 4 Thermodynamics and barriers for decomposition of H_2N–NO into N_2 and H_2O. Thermodynamics are given in black and (parentheses) and kinetic barriers in red and [brackets]. All energies were computed with CCSD(T)/cc-pVQZ and given in kcal mol^{-1}.

The most difficult step *en route* to forming H_2O and N_2 is the isomerization of the *trans*-hydroxydiimide **C** to *cis*-hydroxydiimide **E** *via* **TS4** with a barrier of 38.5 kcal mol^{-1}. However, if the hydroxyl group first rotates to position the hydroxyl proton away from the rest of the molecule the barrier to *trans*/*cis* isomerization drops slightly to 36.1 kcal mol^{-1}. Elimination of H_2O can proceed through **TS7** with a barrier of 18.2 kcal mol^{-1}. Fig. 5 shows the identical reaction as in Fig. 4, but the nitrosamine was placed in the copper-exchanged zeolite

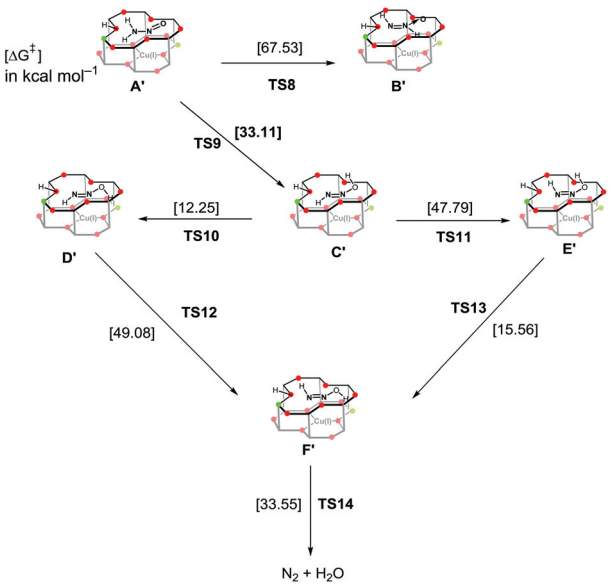

Fig. 5 Reaction barriers in kcal mol^{-1} for generating N_2 and H_2O from H_2NNO when H_2NNO interacts with the zeolite.

matrix. Interestingly, all reaction barriers increase significantly as H-bonding interactions between the nitrosamine protons and zeolite oxygen atoms decrease the mobility of the protons and, as a result, make each respective step of the catalysis more difficult as enumerated in Fig. 5. Thus, the zeolite does not catalyze the decomposition of nitrosamine on its own, but it stabilizes it and inhibits decomposition.

Fundamentally, the somewhat unexpected results discussed above is plausible, since the decomposition of the nitrosamine is governed by proton movement. Thus, we must consider a different role that the zeolite may play: instead of simply stabilizing the nitrosamine by offering hydrogen-bond acceptor sites, the zeolite may act as a proton reservoir and expose Brønsted acid sites that are accessible to the nitrosamine substrate. In particular, the nitrosammonium species that will be formed necessarily when NO reacts with ammonia, will readily provide a proton that the zeolite may reroute to a different site of the molecule mimicking the role of a general Brønsted acid catalyst. Specifically, the excess proton of the nitrosammonium intermediate **4** may be used to significantly lower the barrier of the *trans*/*cis* isomerization step. Our calculations show that the zeolite-bound proton may be transferred to the nitrosamine oxygen atom to give **14** with a barrier of only 7.9 kcal mol^{-1}. The zeolite may subsequently replace its acidic proton by abstracting one of the N-bound protons from **14** to yield the *cis*-hydroxydiimide species **15**, which is nearly isoenergetic with **14**, as illustrated in Fig. 6. These two steps combined yield the *cis* conformation of the hydroxydiimide intermediate completely avoiding the high-barrier *trans*/*cis* isomerization step. The final step for generating N_2 and H_2O is also a proton transfer process and its barrier can also be lowered significantly with the assistance of the zeolite framework. The hydroxyl group on the hydroxydiimide can abstract the zeolite-bound proton to produce water, while another framework oxygen atom from the zeolite may act as a Brønsted base and accept a proton from the remaining N_2H^+ fragment. This proton-shuttling occurs in a concerted fashion through an 8-membered ring transition state that is illustrated in Fig. 6. This acid-catalyzed mechanism enabled by the zeolite facilitates the production of N_2 and H_2O from H_2NNO with a barrier of only 13.8 kcal mol^{-1}, compared to 36.1 kcal mol^{-1} found in the putative uncatalyzed reaction.

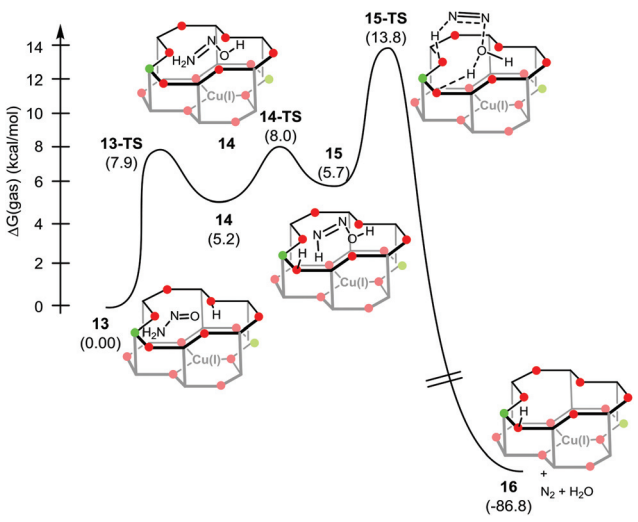

Fig. 6 Mechanism of zeolite-assisted production of N_2 and H_2O from H_2NNO.

Once N_2 and H_2O dissociate, the catalyst can enter the oxidation half cycle of the reaction to regenerate the initial Cu(II) complex **1** from the Cu(I) species **5**. Several potential substrates must be considered for binding to Cu(I), *i.e.*, NO, NH_3, and O_2, which is present in excess under standard SCR conditions. At the onset, there is no conceptual guidance on which sequence of substrate binding should be followed or what the subsequent mechanistic tasks should be. Thus, we have evaluated an exhaustive number of possibilities and compared their energies, while examining the resulting structures to understand the general governing principles of how the Cu(I)-site inserted in the zeolite matrix interacts with the available substrate molecules. Whereas this search was by no means complete, many of the plausible binding scenarios involving various binding sites and binding geometries from a chemically intuitive sense have been explored, and the most viable pathways are summarized in Fig. 7.

Binding of NO and NH_3 to produce **6** and **7** should be competitive as each process is downhill by 10.9 and 10.4 kcal mol^{-1}, respectively. The addition of O_2, however, to give intermediate **8** is uphill by 9.6 kcal mol^{-1} from intermediate **5**. The O_2 molecule is bound in an η^1-fashion in **8** and a significant amount of Mulliken spin density is found on each of the oxygen atoms with 0.777 and 0.944, respectively, compared to 0.249 on Cu. This spin distribution suggests that no electron transfer has taken place upon binding the triplet dioxygen and copper maintains its +I oxidation state in the dioxygen adduct complex. The notable energy penalty for the addition of O_2 indicates that the O_2 must be added after NO or NH_3 binds to Cu. A second substrate binding event on the copper site can generate either **7A**, **8A**, or **8B**. Whereas the ammonia/nitrosyl complex **7A** is most favorable, it lies only 10.0 kcal mol^{-1} lower in energy than **8A** suggesting that an equilibrium should be established between all of the possible adduct structures. Because the nitrosyl ligand in **7A** is bound as a radicaloid species rather than a cation, there is not a sufficient driving force for forming a nitrosamine species as was seen in the reduction half-reaction cycle. Therefore, we considered **8A** as the most viable intermediate for continuing the catalytic cycle. The reoxidation of Cu(I) to Cu(II) has been proposed previously to require both NO and O_2 in order to proceed.[42] Moreover, as **8A** is consumed as the rest of oxidation half-reaction progresses, the equilibrium should shift to replenish **8A** *via* Le Châtelier's principle.

In **8A**, the Cu ion is bound in square pyramidal geometry where it is coordinated to three framework oxygens from the zeolite lattice and an η^1-superoxyl ligand and an anionic nitrosyl moiety. The anionic designation of the nitrosyl moiety is assigned based on the highly bent ∠Cu–N–O angle of 120.6°

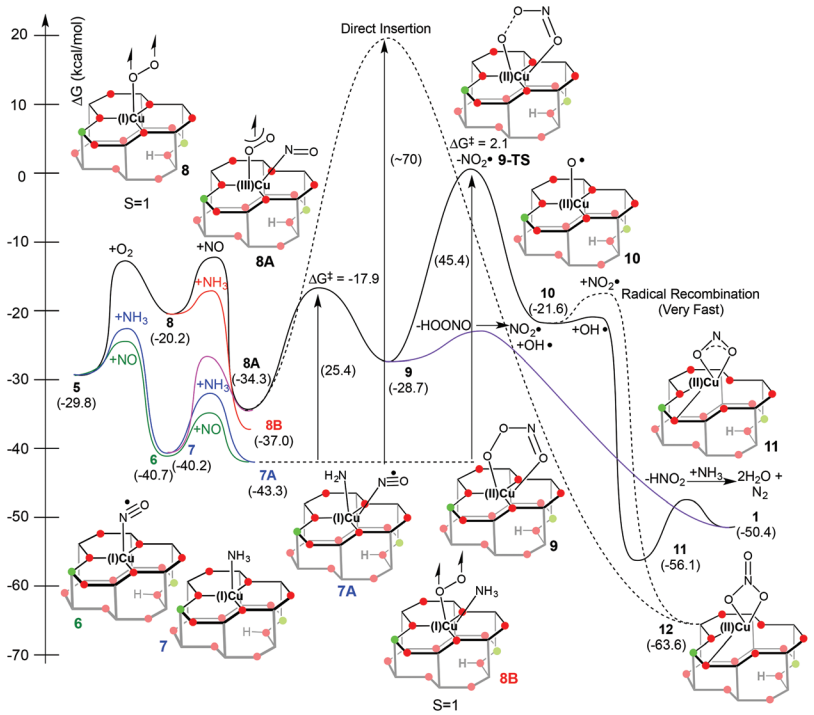

Fig. 7 Mechanism for N_2 formation in oxidation half-cycle. Relative energies in kcal mol^{-1} are given in parenthesis.

along with the minimal spin density found on the nitrosyl fragment (−0.133 on N and −0.074 on O). The Mulliken spin density has also been reduced on the O_2 fragment from 0.777 and 0.944 on the two oxygen atoms in **8** to 0.537 and 0.652 in **8A** indicating that the O_2 fragment has been reduced to a superoxide. Taken with the spin density of only 0.014 on Cu, the calculations suggest that the binding of NO occurs as an oxidative addition with the metal oxidation state changing from Cu(I) to Cu(III) in order to accommodate the five-coordinate geometry around the metal center.

We examined several pathways for inserting the nitrosyl ligand into the O–O bond in order to form the Cu(II)–nitrate complex **12**. Despite significant efforts we were unable to find a well-defined transition state for the direct insertion pathway. Based on a careful scan of the potential energy surface, we estimate that the barrier to the direct insertion will be approximately 70 kcal mol^{-1} as shown in dashed line in Fig. 7. While this number is only an estimate, we do not expect that inserting the nitrosyl directly into the strong O–O bond possessing double bond character is likely. Moreover, only a very small amount of N_2O is typically observed experimentally.[46] As N_2O would likely be produced as a decomposition product after the Cu–bound nitrate is released from **12**, the possibility of undergoing this reaction trajectory seems remote.

Our calculations located an interesting intermediate **9**, a κ^2-bound peroxynitrite species, where the nitrosyl becomes bound through oxygen rather than nitrogen and a bond is formed between the nitrosyl and O_2 ligand to form a 5-member metallacycle. This metallacycle is only 5.6 kcal mol^{-1} higher in energy than **8A**. We found that the formation of the metallacycle has a barrier of 16.4 kcal mol^{-1} in reference to **8A**. However, as **8A** is in equilibrium with several other species, we must take the lowest energy intermediate as the reference point. Therefore, the barrier to formation of the peroxynitrite intermediate **9** is estimated as 25.4 kcal mol^{-1} taking species **7A** as the reference point. As the nitrosyl fragment becomes O-bound in **9**, the nitrosyl must first dissociate as NO˙ from copper, reducing copper from Cu(III) to Cu(II) in the process. Subsequently, the superoxide fragment may undergo a radical recombination reaction with the nitrosyl radical, which is located on the nitrogen atom, to form a new N–O bond.

Once the metallacycle intermediate **9** is formed, it is necessary to break the O–O single bond of the peroxynitrite in order to release the $^{\bullet}NO_2$ radical leaving a Cu(II)–oxyl radical complex **10** behind. As this step must also be referenced to **7A**, we estimate the barrier to be about 45.4 kcal mol^{-1}, which suggests that $^{\bullet}NO_2$ cleavage and release should be the rate-determining step for the reaction. Whereas this barrier is difficult to overcome, it should be accessible at the elevated temperatures of the SCR reaction. It is possible that the incipient $^{\bullet}NO_2$ radical may recombine with the oxyl radical to form the Cu–nitrate **12**, but given the substantially higher concentration of NO˙ in the reaction, a radical recombination reaction to form the κ^2-Cu–nitrite intermediate **11** seems more likely. If the reaction to form the nitrato species **12** were to proceed, reactions between NO and nitrate to give NO_2 have been observed in SCR catalysis.[59,60]

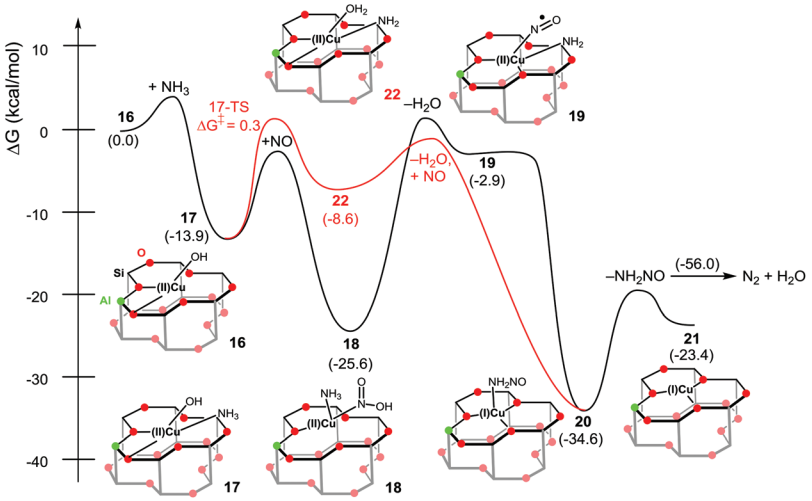

Fig. 8 Reduction half-cycle using a d6r unit doped with **1** aluminate site and hydroxide to compensate the additional charge of the Cu(II) ion.

In order to generate the final products N_2 and H_2O, the Cu-bound nitrate may interact with a proximal Brønsted acid site on the zeolite or another nearby acid such as NH_4^+ to release HNO_2, which may then interact with ammonia to decompose into two equivalents of H_2O and one equivalent of N_2 and restoring the original Cu(II) intermediate **1**. The thermodynamics of releasing nitric acid from **11** are uphill by 5.6 kcal mol^{-1}. This slight cost, however, is more than compensated for when the subsequent reaction with NH_3 takes place, which we calculate to be favorable by 73.9 kcal mol^{-1}.

Our calculations suggest that cleavage of the O–O bond of the peroxynitrite intermediate **9** and subsequent $^{\bullet}NO_2$ release is likely the rate-determining transition state in the mechanism. However, this high energy step might be avoided by binding a proton to the peroxynitrite moiety to generate peroxynitrous acid, which dissociates from Cu as shown in the purple pathway in Fig. 7. High level calculations have shown that the homolysis of HOONO into $^{\bullet}NO_2$ and $^{\bullet}OH$ has a barrier of about 18–19 kcal mol^{-1}.[61,62] The two radicals are only weakly coupled and the mechanism can be considered to be fully dissociative. In solution, the confines of a solvent cage may facilitate recombination of the two radicals, but they are likely to remain dissociated in the gas phase. The hydroxyl radical may react further aided by the high concentration of NO to form HNO_2, which can subsequently decompose to N_2 and H_2O upon reacting with NH_3. Dissociation of the peroxynitrous acid from **9** regenerates **1** to close the catalytic cycle. With the release of peroxynitrous acid, the next step involves the formation of the N–O bond accompanied by the oxidation of NO by O_2 to give the peroxynitrite intermediate **9**. The calculated barrier to this step is 25.4 kcal mol^{-1}. This calculated activation energy is somewhat higher than the measured apparent activation energy for the oxidation half-cycle of about 17 kcal mol^{-1}.[42] The reported experimental value probably takes into account other factors such as the adsorption energy of the reactants as described by the Langmuir isotherm, which are not included in the DFT calculations.[42]

We have also probed an alternative model shown in Fig. 8, where the second aluminate site has been replaced by a silicon atom and instead the Cu(II) ion is supported by a bound hydroxide (^{-}OH) ion. The initial Cu(II)–OH complex **16** can bind NH_3 with a free energy of binding of 13.9 kcal mol^{-1}. The resulting [Cu(II)–(NH_3)(OH)] complex **17** can potentially bind a nitrosyl ligand, which may insert into the Cu–OH bond to form intermediate **18** in a reaction that is downhill energetically by 12.7 kcal mol^{-1}. Intermediate **18** can transfer a proton between ammonia and nitrous acid to release water and generate the [Cu(NO)(NH_2)] intermediate **19**. The calculated driving force between intermediate **19** and the nitrosamine intermediate **20** is 31.7 kcal mol^{-1} and, thus, it is expected to lead to a rapid addition of the nitrosyl fragment to the amido moiety. Alternatively, the ammine ligand in intermediate **17** can transfer a proton to the hydroxyl fragment to give [Cu(II)–(NH_2)(OH_2)] intermediate **22**. This intermediate lies 5.3 kcal mol^{-1} higher in energy than **17** and the barrier to proton transfer between the ammine and hydroxyl moiety is calculated to be 14.2 kcal mol^{-1} higher in energy than **17**. Dissociation of water followed by rapid reaction of the amido ligand with free NO yields the nitrosamine species **20**. A scan of the potential energy surface describing the approach of NO to the amido ligand to form the N–N bond of the nitrosamine suggests that this process may be barrierless on the electronic potential energy surface. The release of the nitrosamine from Cu is calculated to be uphill by 11.2 kcal mol^{-1}, but the thermodynamic driving force for the decomposition of the nitrosamine into N_2 and H_2O is 56.0 kcal mol^{-1}. As in the 2-aluminum model in Fig. 2, an acidic proton may be recruited to help in a zeolite-assisted decomposition of the nitrosamine to release N_2 and H_2O with a maximum barrier of 13.8 kcal mol^{-1}. The remaining Cu(I) ion can successively bind NO,

NH_3, or O_2 to begin the oxidation half-reaction cycle as illustrated in Fig. 7 with the 2-aluminate models.

Conclusions

We have examined various mechanistic possibilities for the reduction of NO on Cu-SSZ-13 in the presence of NH_3 and O_2 using both one and two-aluminum doped zeolite cluster models. Our calculations indicate that N_2 can be produced in the reduction half-reaction cycle through a nitrosamine intermediate. The copper-exchanged chabazite has two key functions to play in this part of the catalytic cycle: (a) the copper site facilitates the generation of NO^+, which is then held in place by the zeolite framework using electrostatic force until it can be attacked by ammonia to give the nitrosamine intermediate. (b) Once nitrosamine is formed, copper retreats by moving to the lower half of the zeolite cage unit. For the further processing of the nitrosamine intermediate, the zeolite acts as a "proton sponge", accepting from and donating to the various intermediates protons as needed to enable general Brønsted acid catalyzed decomposition of the nitrosoamine to N_2 and H_2O.

N_2 production in the oxidation half-reaction proceeds through a Cu-peroxynitrite metallacycle. Release of $^{\bullet}NO_2$ from this metallacycle is the most likely candidate for the rate-determining step of the mechanism and is followed by rapid radical recombination of $NO^{\bullet}$ with the incipient Cu–$O^{\bullet}$. The resulting Cu–NO_2 species can react with nearby acids to generate HNO_2 that can subsequently react with NH_3 to yield N_2 and H_2O. To the best of our knowledge, this is the first proposal of the complete catalytic cycle of the selective catalytic reduction of NO that provides both detailed structural and energetic information. The computed results are correlated to plausible function of the catalyst. Whereas the calculated numbers are important, they are not taken simply as a number, but are scrutinized to be rationalized in a chemically intuitive sense. This generalization is important, as they outline what the mechanistic function of each step and what each step accomplishes ultimately. Such conceptual analysis of the proposed catalytic cycle is key for further improving the catalyst in future work. Thus, this investigation provided a detailed mechanistic foundation, upon which future optimization strategies of the Cu-SSZ-13 catalyst can be derived and tested.

Acknowledgements

We thank Institute for Basic Science (IBS-R10-D1) in Korea, the Research Corporation (Scialog Award to M.-H. B.) and the BASF Corporation for support of this work.

References

1 P. Granger and V. I. Parvulescu, *Chem. Rev.*, 2011, **111**, 3155.
2 R. Burch, *Catal. Rev.*, 2004, **46**, 271.
3 S. Brandenberger, O. Krocher, A. Tissler and R. Althoff, *Catal. Rev.*, 2008, **50**, 492.
4 S. Roy and A. Baiker, *Chem. Rev.*, 2009, **109**, 4054.
5 E. Tronconi, I. Nova, C. Ciardelli, D. Chatterjee, B. Bandl-Konrad and T. Burkhardt, *Catal. Today*, 2005, **105**, 529.
6 D. A. Peña, B. S. Uphade and P. G. Smirniotis, *J. Catal.*, 2004, **221**, 421.
7 G. Busca, L. Lietti, G. Ramis and F. Berti, *Appl. Catal., B*, 1998, **18**, 1.
8 L. Casagrande, L. Lietti, I. Nova, P. Forzatti and A. Baiker, *Appl. Catal., B*, 1999, **22**, 63.
9 E. Tronconi, I. Nova, C. Ciardelli, D. Chatterjee and M. Weibel, *J. Catal.*, 2007, **245**, 1.
10 C. Ciardelli, I. Nova, E. Tronconi, D. Chatterjee, B. Bandl-Konrad, M. Weibel and B. Krutzsch, *Appl. Catal., B*, 2007, **70**, 80.
11 J. M. García-Cortés, J. Pérez-Ramírez, M. J. Illán-Gómez, F. Kapteijn, J. A. Moulijn and C. S.-M. de Lecea, *React. Kinet. Catal. Lett.*, 2000, **70**, 199.
12 M. Iwamoto, H. Furukawa, Y. Mine, F. Uemura, S. Mikuriya and S. Kagawa, *J. Chem. Soc., Chem. Commun.*, 1986, **16**, 1272.
13 M. Iwamoto, H. Yahiro, Y. Mine and S. Kagawa, *Chem. Lett.*, 1989, **18**, 213.
14 M. Iwamoto, H. Yahiro, K. Tanda, N. Mizuno, Y. Mine and S. Kagawa, *J. Phys. Chem.*, 1991, **95**, 3727.
15 X. Yang, Z. Wu, M. Moses-Debusk, D. R. Mullins, S. M. Mahurin, R. A. Geiger, M. Kidder and C. K. Narula, *J. Phys. Chem. C*, 2012, **116**, 23322.
16 I. Bull, W.-M. Xue, P. Burk, R. S. Boorse, W. M. Jaglowski, G. S. Koermer, A. Moini, J. A. Patchett, J. C. Dettling and M. T. Caudle, *US Pat.*, 7601662, 2009.
17 U. Deka, A. Juhin, E. A. Eilertsen, H. Emerich, M. A. Green, S. T. Korhonen, B. M. Weckhuysen and A. M. Beale, *J. Phys. Chem. C*, 2012, **116**, 4809.
18 S. T. Korhonen, D. W. Fickel, R. F. Lobo, B. M. Weckhuysen and A. M. Beale, *Chem. Commun.*, 2011, **47**, 800.
19 J. H. Kwak, H. Zhu, J. H. Lee, C. H. F. Peden and J. Szanyi, *Chem. Commun.*, 2012, **48**, 4758.
20 F. Giordanino, P. N. R. Vennestrom, L. F. Lundegaard, F. N. Stappen, S. Mossin, P. Beato, S. Bordiga and C. Lamberti, *Dalton Trans.*, 2013, **42**, 12741.
21 V. F. Kispersky, A. J. Kropf, F. H. Ribeiro and J. T. Miller, *Phys. Chem. Chem. Phys.*, 2012, **14**, 2229.
22 D. W. Fickel, E. D'Addio, J. A. Lauterbach and R. F. Lobo, *Appl. Catal., B*, 2011, **102**, 441.
23 Q. Ye, L. Wang and R. T. Yang, *Appl. Catal., A*, 2012, **427–28**, 24.
24 F. Gao, E. D. Walter, N. M. Washton, J. Szanyi and C. H. F. Peden, *ACS Catal.*, 2013, **3**, 2083.
25 J. H. Kwak, R. G. Tonkyn, D. H. Kim, J. Szanyi and C. H. F. Peden, *J. Catal.*, 2010, **275**, 187.
26 J. H. Kwak, D. Tran, J. Szanyi, C. F. Peden and J. Lee, *Catal. Lett.*, 2012, **142**, 295.

27 J. S. McEwen, T. Anggara, W. F. Schneider, V. F. Kispersky, J. T. Miller, W. N. Delgass and F. H. Ribeiro, *Catal. Today*, 2012, **184**, 129.
28 J. H. Kwak, J. H. Lee, S. D. Burton, A. S. Lipton, C. H. F. Peden and J. Szanyi, *Angew. Chem., Int. Ed.*, 2013, **52**, 9985.
29 F. Göltl and J. Hafner, *J. Chem. Phys.*, 2012, **136**, 064501.
30 F. Göltl and J. Hafner, *J. Chem. Phys.*, 2012, **136**, 064502.
31 F. Göltl and J. Hafner, *J. Chem. Phys.*, 2012, **136**, 064503.
32 F. Göltl, R. E. Bulo, J. Hafner and P. Sautet, *J. Phys. Chem. Lett.*, 2013, **4**, 2244.
33 D. W. Fickel, J. M. Fedeyko and R. F. Lobo, *J. Phys. Chem. C*, 2010, **114**, 1633.
34 S. A. Bates, A. A. Verma, C. Paolucci, A. A. Parekh, T. Anggara, A. Yezerets, W. F. Schneider, J. T. Miller, W. N. Delgass and F. H. Ribeiro, *J. Catal.*, 2014, **312**, 87.
35 E. Borfecchia, K. A. Lomachenko, F. Giordanino, H. Falsig, P. Beato, A. V. Soldatov, S. Bordiga and C. Lamberti, *Chem. Sci.*, 2015, **6**, 548.
36 U. Deka, I. Lezcano-Gonzalez, B. M. Weckhuysen and A. M. Beale, *ACS Catal.*, 2013, **3**, 413.
37 F. Gao, E. D. Walter, M. Kollar, Y. Wang, J. Szanyi and C. H. F. Peden, *J. Catal.*, 2014, **319**, 1.
38 F. Gao, J. H. Kwak, J. Szanyi and C. F. Peden, *Top. Catal.*, 2013, **56**, 1441.
39 F. Giordanino, E. Borfecchia, K. A. Lomachenko, A. Lazzarini, G. Agostini, E. Gallo, A. V. Soldatov, P. Beato, S. Bordiga and C. Lamberti, *J. Phys. Chem. Lett.*, 2014, **5**, 1552.
40 F. Gao, E. D. Walter, E. M. Karp, J. Luo, R. G. Tonkyn, J. H. Kwak, J. Szanyi and C. H. F. Peden, *J. Catal.*, 2013, **300**, 20.
41 S. T. Korhonen, D. W. Fickel, R. F. Lobo, B. M. Weckhuysen and A. M. Beale, *Chem. Commun.*, 2011, **47**, 800.
42 T. V. W. Janssens, H. Falsig, L. F. Lundegaard, P. N. R. Vennestrøm, S. B. Rasmussen, P. G. Moses, F. Giordanino, E. Borfecchia, K. A. Lomachenko, C. Lamberti, S. Bordiga, A. Godiksen, S. Mossin and P. Beato, *ACS Catal.*, 2015, **5**, 2832.
43 J. Szanyi, J. H. Kwak, H. Zhu and C. H. F. Peden, *Phys. Chem. Chem. Phys.*, 2013, **15**, 2368.
44 R. Zhang, J.-S. McEwen, M. Kollár, F. Gao, Y. Wang, J. Szanyi and C. H. F. Peden, *ACS Catal.*, 2014, **4**, 4093.
45 D. E. Doronkin, M. Casapu, T. Günter, O. Müller, R. Frahm and J.-D. Grunwaldt, *J. Phys. Chem. C*, 2014, **118**, 10204.
46 D. W. Crandell, H. Zhu, X. Yang, J. Hochmuth and M.-H. Baik, *Inorg. Chim. Acta*, 2015, **430**, 132.
47 C. Paolucci, A. A. Verma, S. A. Bates, V. F. Kispersky, J. T. Miller, R. Gounder, W. N. Delgass, F. H. Ribeiro and W. F. Schneider, *Angew. Chem., Int. Ed.*, 2014, **53**, 11828.
48 R. G. Parr and W. Yang, *Density Functional Theory of Atoms and Molecules*, Oxford University Press, New York, 1989.
49 T. Ziegler, *Chem. Rev.*, 1991, **91**, 651.
50 Jaguar, version 8.1 Schrödinger, LLC, New York, NY, 2013.
51 J. P. Perdew, K. Burke and M. Ernzerhof, *Phys. Rev. Lett.*, 1996, **77**, 3865.
52 W. J. Hehre, R. Ditchfield and J. A. Pople, *J. Chem. Phys.*, 1972, **56**, 2257.
53 P. J. Hay and W. R. Wadt, *J. Chem. Phys.*, 1985, **82**, 270.
54 P. J. Hay and W. R. Wadt, *J. Chem. Phys.*, 1985, **82**, 299.
55 T. H. Dunning Jr., *J. Chem. Phys.*, 1989, **90**, 1007.
56 K. Raghavachari, G. W. Trucks, J. A. Pople and M. Head-Gordon, *Chem. Phys. Lett.*, 1989, **157**, 479.
57 F. Neese, *WIREs Comput. Mol. Sci.*, 2012, **2**, 73.
58 Y. Zhao and D. G. Truhlar, *Theor. Chem. Acc.*, 2008, **120**, 215.
59 C. Ciardelli, I. Nova, E. Tronconi, D. Chatterjee and B. Bandl-Konrad, *Chem. Commun.*, 2004, 2718.
60 A. Grossale, I. Nova, E. Tronconi, D. Chatterjee and M. Weibel, *J. Catal.*, 2008, **256**, 312.
61 Y. Zhao, K. N. Houk and L. P. Olson, *J. Phys. Chem. A*, 2004, **108**, 5864.
62 D. A. Dixon, D. Feller, C.-G. Zhan and J. S. Francisco, *J. Phys. Chem. A*, 2002, **106**, 3191.